– №12. – С.16–20. **4.** *Биргер И.А., Пановко Я.Г.* Прочность, устойчивость, колебания: Справочник. – М.: Машиностроение,1968. – 520с. **5.** ГОСТ 21354-87. Передачи зубчатые цилиндрические эвольвентные внешнего зацепления. Расчет на прочность. – Введен 01.01.1989. – М.: Изд-во стандартов, 1989. – 76с. **6.** *Ковальский Б.С.* Расчет деталей на местное сжатие. – Харьков: Изд-во ХВВКИУ, 1967. – 156с. **7.** *Загребельный В.Н., Устиненко А.В.* Определение контактных напряжений в двухпараметрических зацеплениях // Механіка та машинобудування. – 1998. – №1. – С.19–21. **8.** *Когаев В.П.* Расчеты на прочность при напряжениях, переменных во времени. – М.: Машиностроение, 1977. – 232с. **9.** *Кириченко А.Ф., Устиненко А.В.* Об определении допускаемых напряжений при расчете зубчатых передач путем математического моделирования усталостных процессов // Вестник НТУ "ХПИ": Сб. научн. трудов. Тем. вып. "Проблемы механического привода". – Харьков, 2004. – №30. – С.39–44.

Поступила в редколлегию 01.04.2013

УДК 539.3

A. ZOLOCHEVSKY, Dr. Sc., NTU “Kharkov Polytechnic Institute”;
A. GALISHIN, Dr. Sc., Institute of Mechanics, National Academy of Sciences of Ukraine;
S. SKLEPUS, Dr., Institute of Mechanical Engineering Problems, National Academy of Sciences of Ukraine;
L. PARKHOMENKO, Kharkov State University of Food Technology and Trade, Kharkov;
V. GNITKO, Dr., Institute of Mechanical Engineering Problems, National Academy of Sciences of Ukraine, Kharkov;
A. KÜHHORN, Dr., Brandenburg Technical University at Cottbus, Germany,
M. KOBER, Dr., Brandenburg Technical University at Cottbus, Germany,
C. LEYENS, Dr., German Aerospace Center, Germany

BENCHMARK CREEP TESTS FOR THERMAL BARRIER COATINGS

Тема цієї статті включає в себе ряд тестів на повзучість та еталонні рішення, які дають можливість перевірити аналіз методом скінченних елементів перерозподілу напружень в теплозахисних покриттях, пов'язаний з комерційними пакетами програмного забезпечення. Чисельні результати були порівняні у тестах з результатами, отриманими іншими методами та іншими авторами. Результати досліджень повзучості показали величини локальних напружень, які корелюють із залишковими напруженнями, визначеними в термічно вирощеному оксиді методом люмінесцентної спектроскопії. Повзучість нікелевих жароміцних сплавів підкладки має сильний вплив на напружений стан і подальше руйнування EB-PVD теплозахисних покриттів. Отримані чисельні результати показують, що майбутні EB-PVD теплозахисні покриття повинні бути розроблені одночасно з нікелевою підкладкою, оскільки ефективність покриття залежить від складу і властивостей підкладки.

Ключові слова: теплозахисне покриття; EB-PVD; повзучість; тест; багатошарова система; напружений стан.

Тема этой статьи включает в себя ряд тестов на ползучесть и эталонные решения, которые дают возможность проверить анализ методом конечных элементов перераспределения напряжений в теплозащитных покрытиях, связан с коммерческими пакетами программного обеспечения. Численные результаты были сравнены в тестах с результатами, полученными другими методами и другими авторами. Результаты исследований ползучести показали величины локальных напряжений, которые коррелируют с остаточными напряжениями, определенными в термически выращенном окисле методом люминесцентной спектроскопии. Ползучесть никелевых жаропрочных сплавов подложки имеет сильное влияние на напряженное состояние и дальнейшее разрушение EB-PVD теплозащитных покрытий. Полученные численные результаты показывают, что будущие EB-PVD теплозащитные покрытия должны быть разработаны одновременно с никелевой подложкой, поскольку эффективность покрытия зависит от состава и свойств подложки.

Ключевые слова: теплозащитное покрытие; EB-PVD; ползучесть; тест; многослойная система; напряженное состояние.

The topic of this paper involves a number of benchmark creep tests and reference solutions that give the possibility to verify the finite element analysis of stress redistribution in thermal barrier coatings related to commercial software packages. The numerical results have been compared in the benchmark tests with the results obtained by other methods and by other authors. The results of creep studies revealed the magnitudes of the local stresses that correlate with the residual stresses determined in the thermally grown oxide by the luminescence spectroscopy method. The creep properties of Ni-based superalloy substrate have strong influence on the stress state and subsequent failure of EB-PVD thermal barrier coatings. The obtained numerical results demonstrate that the future EB-PVD thermal barrier coatings should be developed simultaneously with the Ni-based superalloy substrate, because the effectiveness of coating is influenced by the composition and properties of the substrate.

Keywords: thermal barrier coating; EB-PVD; creep; benchmark; multilayer system; stress

1. Introduction. For structures operating in harsh environments up to temperatures in excess of 900 °C, a coating may be applied to protect the material from direct exposure to the environment. In this way, protective coatings are required for both environmental protection and thermal insulation of the structural material [1-3]. Thus, a protective coating can substantially improve at high temperatures the application potential of gas turbine blades of aircraft engines made out of Ni-based superalloys.

The coating system for Ni-based superalloy substrate has a very complex structure and generally consists of several intermediate layers with a spatial variance in properties [4]. Conventional Pt modified aluminides or MCrAlY coatings (M = Ni and/or Co) are suitable as protective coatings for Ni-based superalloys due to the excellent chemical and physical compatibility with the substrate [5]. These metallic coatings are applied to the Ni-based superalloy substrates either by electron beam- physical vapor deposition (EB-PVD) in the case of the MCrAlY or by chemical vapour deposition for the Pt modified aluminide [6]. They are improving remarkably the oxidation resistance of Ni-based superalloys. In the following, the coated substrate was pre-oxidized to form an alumina scale (Al_2O_3) [7]. A MCrAlY (or Pt modified aluminide) layer serves also as a suitable bond coat (BC) for yttria partially stabilized zirconia (ZrO_2 – 7-8 wt % Y_2O_3) due to the good adherence of the zirconia top coat (TC) to the alumina scale. The yttria partially stabilized zirconia (7-8 YSZ) is deposited on the pre-coated Ni-based superalloy substrate using the EB-PVD technique, and it serves as excellent thermal barrier coating (TBC). The usage of approximately 200 μm thick ceramic EB-PVD TBC on the surface of a gas turbine blade gives rise to the surface temperature re-

duction up to 150 °C [8]. The extremely low thermal conductivity and good phase stability make a YSZ the most successful ceramic top layer, when combined with a metallic interlayer. As the BC oxidizes, oxygen diffuses through Al_2O_3 to react at the metal-oxide interface and to create more oxide. Thus, a multilayer TBC system includes the Ni-based superalloy substrate, the BC, the TC and the thermally grown oxide (TGO).

Degradation of the TBC systems over time can be investigated experimentally at laboratory conditions under thermal cyclic loading using the burner rig testing [9, 10]. Typical sample geometries are pins, plates, disks or turbine blades. A number of factors related to the numerous phenomena can affect damage growth and lifetime reduction of the TBC systems. In this way, the mechanisms of thermal, chemical, mechanical and structural degradation of multilayer coating systems involving Ni-based superalloys have been identified and studied [11-13]. In this regard, special attention is given to the consideration of high temperature oxidation [14-17], creep [18-20], fatigue [21-23] and wear [8, 24, 25] occurring in TBC systems.

Polycrystalline materials in TBC systems operating at high temperatures for a prolonged period of time exhibit creep deformation considered as a time-dependent irreversible deformation process. Even at the primary and secondary stages of the creep deformation, dislocations, impurity atoms and voids accumulate at the grain facets of metal and ceramic multilayers to form a cavitation [26, 27]. As microscopic grain boundary cavities get larger and coalesce, dislocations, impurities and voids move out to grain boundaries, and microcracks along the grain boundaries start to be formed. Growth and coalescence of these microcracks at the grain boundaries of metal and ceramic multilayers occur in the tertiary stage of the creep process with the formation of macrocracks with some preferential orientation, often, directed perpendicular to the maximum principal stress, and, finally, with the creep rupture of a TBC system. Thus, creep changes the microstructure of metal and ceramic multilayers of TBC systems by introducing dislocations, impurities and voids in the initial stages of deformation, microscopic cavities in the following, and microcracks in the final stage of the creep process, all of them, at the grain faces with some preferential orientation. Furthermore, the growth rate of pre-existing flaws, as well as, the growth of the irreversible formation of a nucleus of the new grain boundary microscopic cavities and microcracks essentially depend on the intensity of the creep process. At the same time, creep deformation of metal and ceramic multilayers in TBC systems is affected by the growth of cavities and microcracks. This influence that begins in the initial stages of the creep deformation, can be observed in the final stage of creep before rupture due to a possible increase of the creep strain rate. The creep rupture case without increase in the creep strain rate can be also observed. Thus, creep deformation and material deterioration in TBC systems due to growth of creep damage occur parallel to each other, and they have a reciprocal effect. Obviously, creep damage growth in metal and ceramic multilayers leads to the degradation of TBC systems over time.

Thus, the functionality and reliability of Ni-based superalloy components with a TBC for automotive, energy and aerospace applications are strongly related to the creep damage

growth and stress redistribution over time in the coating system. A methodology for the durability analysis of multilayer coating systems with Ni-based superalloy substrate is needed that complements experimental procedures for the evaluation of coatings.

There are various sources of stresses in coatings [28]:

a) Thermal induced stresses resulting from temperature changes and differences of the coefficient of thermal expansion of coating layers and substrate material.

b) Stresses resulting from coating growth. In this case it is necessary to distinguish between intrinsic growth stresses and geometrically-induced stresses. Intrinsic growth stresses are due to oxidation; chemical reactions, phase transformations, energetic particle bombardment, etc.

c) Stresses due to the deformation of the coating systems under the applied loading and environmental influences.

A small amount of studies on time dependent stresses under creep conditions in TBC systems involving Ni-based superalloy substrate are available in the literature. In this regard, it is necessary to address the following questions. First, creep studies existing in the literature are related to the modeling of the burner rig tests with simple sample geometries like pins, plates, disks, but not turbine blades. Second, creep analysis of TBC systems with consideration of a thermal gradient over the sample wall is scarce. Third, stresses from the creep curves used for the determination of material parameters in the creep constitutive equations must be identical with the original ones which occur in TBC systems. In the opposite case being considered, for example, in [29], the effect of creep on the stress state in a TBC system cannot be identified by the numerical analysis. Fourth, most studies do not involve creep of all layers. Hence, it is assumed that a number of layers in a TBC system are deformed only thermoelastically while others also demonstrate creep deformation [30-39]. Furthermore, a high degree of numerical boundary stiffness has been introduced in [40] instead of the substrate. Fifth, creep of all system constituents was taken into account in several publications [41-43], however, without consideration of the applied forces. Finally, there is no comparative study of the creep behavior of TBC systems using results obtained by various authors or by different methods.

The concept of benchmarks is becoming increasingly important in computational structural analysis [44]. By using benchmark tests and reference solutions researchers have the possibility to verify their numerical results related to the finite element code and commercial software packages (ANSYS, ABAQUS, ADINA). Several benchmark creep problems are considered in [45-49]. In the present paper, attention is given to the benchmark creep tests together with the reference solutions for the TBC systems involving Ni-based superalloy substrate. This study does not consider degradation of TBC systems induced by high temperature oxidation, ratcheting, fatigue and wear. These issues will be a subject for future research.

2. DLR sample for testing. The burner rig tests are less time consuming and cost intensive than gas turbine engine tests [9, 50]. Hence, the gas burner facilities give the possibility to evaluate the behavior of TBC systems at the laboratory conditions under thermomechanical cyclic loading. Different sample geometries like pins, plates or disks

were used, i.e. there is no single point of view on the burner rig testing.

In the present paper, we take into account that mutiaxial stress states in turbine blades can be generated due to the thermal gradients over the blade wall, as well as, due to centrifugal forces. Special attention is paid to the sample geometry and testing procedure accepted at the German Aerospace Center (DLR) [22, 50, 51]. Hence, in order to study the degradation of TBC systems, which may oc-cur in-service and limit the performance of turbine blades, the test specimen (Fig. 1) was subjected in the DLR laboratory to conditions, which simulate the in-service condition as close as possible. The TBC system includes Ni-based superalloy substrate, the BC, the TGO and the TC. The proportions of these layers in Fig. 1 do not reflect their actual sizes. Testing of the multilayer tubular specimen realizes cyclic thermal and mechanical loading including a thermal gradient over the specimen wall. An applied mechanical loading by a force N reproduces the centrifugal force acting on the turbine blade. In general, the temperature T (Fig. 2) on the inner and outer surfaces of the tubular specimen and the load N can act over time under an in-phase and out-of-phase loading mode [52]. A heating period t_1, a dwell time $t_2 - t_1$ and a cooling period $t_3 - t_2$ in the applied test cycle for the surface temperatures should be introduced in order to represent the degradation of TBC systems during an entire flight of a jet engine. It is possible to accept for the DLR cycle [50] approximately $t_1 = 30$ s, $t_2 - t_1 = 2$ min and $t_3 - t_2 = 15$ s.

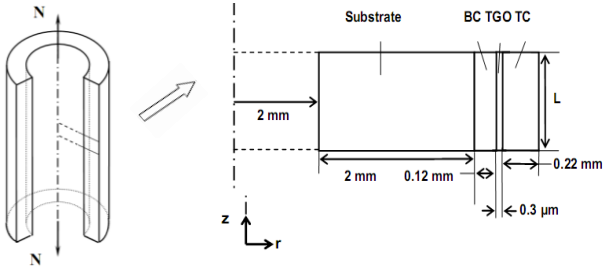

Fig. 1 – Schematic representation of the TBC system [50]

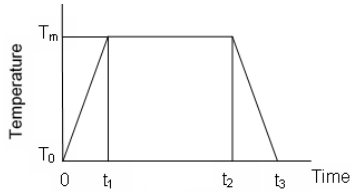

Fig. 2 – The cycle of temperature

3. Modeling. The deformation of the test multilayer hollow cylinder (Fig. 1) with the inner and outer radii a and b after start up at time instants $t \geq t_1$ is considered. We do not need to take creep during a heating period into account. The cylinder is sufficiently long in the axial direction compared to its diameter. The test specimen is subjected to an axial load N, as well as, to a temperature $T_m = T_a$ on the inside and $T_m = T_b$ on the outside of its walls.

In contrast to many experimental investigations of TBC systems, indications of rumpling of the TGO were not well pronounced, and an increasing waviness of the TGO over time was not observed experimentally in [53]. Following these experimental results, the modeling of TBC systems in the present paper is given without considera-

tion of rumpling and waviness of the TGO in the cylindrical coordinate system (r,θ,z), as shown in Fig. 1. Here *r* is the radial coordinate, θ corresponds to the circumferential direction, and *z* is the axial coordinate. The temperature in a specimen can be assumed to be independent of the coordinates θ and *z*, and, therefore, it will be a function of the radial coordinate *r* and the time *t* only, i.e. $T=T(r,t)$.

The stress state in the multilayer cylinder under study will be analyzed under assumptions of generalized plane strain and symmetry about the axis *z*. In this regard, there are three nonzero components of strain $\varepsilon_r,\varepsilon_\theta,\varepsilon_z$ and three nonzero components of stress $\sigma_r,\sigma_\theta,\sigma_z$. The components of strain are assumed to be the sum of the elastic part, thermal part and creep part, i.e.

$$\varepsilon_r=\varepsilon_r^e+\varepsilon_r^T+\varepsilon_r^c;\quad \varepsilon_\theta=\varepsilon_\theta^e+\varepsilon_\theta^T+\varepsilon_\theta^c;\quad \varepsilon_z=\varepsilon_z^e+\varepsilon_z^T+\varepsilon_z^c. \tag{1}$$

The components of the elastic strain can be defined by the generalized Hooke's law for isotropic materials in such a form

$$\varepsilon_r^e=\frac{1}{E}\left[\sigma_r-\nu(\sigma_\theta+\sigma_z)\right];\ \varepsilon_\theta^e=\frac{1}{E}\left[\sigma_\theta-\nu(\sigma_r+\sigma_z)\right];\ \varepsilon_z^e=\frac{1}{E}\left[\sigma_z-\nu(\sigma_r+\sigma_\theta)\right], \tag{2}$$

where *E* is the Young's modulus, and ν is the Poisson's ratio. The components of the thermal strain can be written as follows

$$\varepsilon_r^T=\varepsilon_\theta^T=\varepsilon_z^T=\alpha(T-T_{\text{ref}}), \tag{3}$$

where α is the thermal expansion coefficient, and T_{ref} is the temperature at the reference state.

The loading conditions under consideration give the possibility to analyze the isotropic creep with time hardening, and without the memory effect and softening [54]. In this regard, the components of the creep strain rate under a multiaxial stress state can be defined as follows [55]

$$\begin{aligned}
\dot{\varepsilon}_r^c&=\frac{3}{2}Amt^{m-1}\sigma_i^{n-1}\left[\sigma_r-\frac{1}{3}(\sigma_r+\sigma_\theta+\sigma_z)\right];\\
\dot{\varepsilon}_\theta^c&=\frac{3}{2}Amt^{m-1}\sigma_i^{n-1}\left[\sigma_\theta-\frac{1}{3}(\sigma_r+\sigma_\theta+\sigma_z)\right];\\
\dot{\varepsilon}_z^c&=\frac{3}{2}Amt^{m-1}\sigma_i^{n-1}\left[\sigma_z-\frac{1}{3}(\sigma_r+\sigma_\theta+\sigma_z)\right],
\end{aligned} \tag{4}$$

where the dot above the symbol denotes the derivative with respect to time t, σ_i is the von Mises equivalent stress, and *A*, *n* and *m* are the temperature dependent material constants.

A number of comments need to be made in reference to Eq. (4). First, the von Mises stress in the present case has the structure

$$\sigma_i = \frac{1}{\sqrt{2}}\sqrt{(\sigma_r - \sigma_\theta)^2 + (\sigma_z - \sigma_\theta)^2 + (\sigma_r - \sigma_z)^2}\ . \qquad (5)$$

Second, the materials under creep conditions are assumed incompressible, and with the same response under tensile and compressive loading types. Third, in the case of uniaxial tension with stress $\sigma_z = \sigma$ =const Eq. (4) transforms to $\dot{\varepsilon}_z^c = Amt^{m-1}\sigma^n$, $\dot{\varepsilon}_r^c = \dot{\varepsilon}_\theta^c = -\frac{1}{2}Amt^{m-1}\sigma^n$. Thus, under uniaxial tension Eq. (4) reflects the approximation of the creep curves in the direction of loading, such as

$$\varepsilon_z^c = At^m\sigma^n\ . \qquad (6)$$

Two different numerical approaches and two in-house developed software packages were used in the present study to find the stresses in TBC systems under creep conditions. The first approach is the variational approach of establishing the basic equations of the generalized plane strain problem under consideration with use of the fourth-order Runge-Kutta-Merson's method of time integration, combined with the Ritz method for solving the creep problem. This approach used earlier [56] for the analysis of a plain stress problem was applied after small modifications without any difficulties to the generalized plane strain problems. The second approach is the application of the refined theory of creep deformation in moderately thick shells of revolution which accounts for nonlinear distribution over their thickness of the components of strain tensor [57, 58] with use of the fourth-order Runge-Kutta-Merson's method of time integration, combined with the discrete orthogonal shooting method of Godunov for the solution of creep problems. Initially, of course, it is necessary to do the comparative study of these two numerical approaches in TBC systems.

4. Reference solution for thin plate. As a first example to verify the two approaches discussed above, the multilayer thin circular plate (Fig. 3) with an inner radius of 2.0 mm and an outer radius of 4.111 mm consisted of Ni-based superalloy substrate, the BC and the TGO is considered [59] instead of a multilayer long cylinder. The TC is ignored for simplicity in the present analysis. The thin plate under study is subjected to the temperatures T_a = 800°C on the inside and T_b = 1000°C on the outside of its walls (Fig. 3).

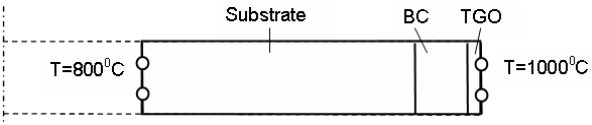

Fig. 3 – The multilayer thin circular plate

The geometrical and material parameters for three layers of the coating system are given in Table 1. Hence, the thickness of the plate is not defined, because

the stress-strain state in the thin plate under consideration was assumed to be the same along the thickness direction, and, thus, this size plays no role for determining stress components under plane stress conditions. The temperature at the reference state was taken as deposition temperature of the coating, i.e. $T_{\text{ref}} = 1000°\text{C}$. In this study, the thermoelastic deformation of the three layers has been taken into account, and creep of the plate is ignored for simplicity.

Table 1 – **Material properties and geometrical dimensions used for the calculations of thermal stresses in a multilayer thin circular plate**

Layer	Elastic modulus (GPa)	Poisson's ratio	Thermal expansion $\times 10^6$ ($°\text{C}^{-1}$)	Thermal conductivity (W/m/°C)	Thickness (mm)
Substrate	150	0.3	16	30	2.0
Bond coat	100	0.3	15	20	0.110
TGO	310	0.2	8	6	0.001

The distribution of the temperature in a plate at the steady state is shown in Fig. 4. It is based on the analytical solution [59] to the Fourier's law for heat transfer with the boundary conditions T= 800 °C at $r = a$ and T= 1000 °C at $r = b$, and the continuity conditions for temperature and heat flux along interfaces. The dimensionless coordinate in the i – th layer of the plate (I = 1, 2 and 3) has been introduced in Fig. 4 as

$$\xi_i = \alpha_i \frac{r - r_{i-1}}{r_i - r_{i-1}} + \sum_{k=0}^{i-1} \alpha_k \ . \qquad (7)$$

Hence, it is assumed that the plate consists of three layers (the substrate, the BC and the TGO) numbered 1, 2 and 3, respectively, $r_i = r_{i-1} + h_i$, $r_0 = a, h_i$ is the thickness of the i – th layer, $r_3 = b$, α_i is the weight coefficient introduced in such a way that $\alpha_0 = 0$, $\alpha_1 = 0.6$, $\alpha_2 = 0.25$ and $\alpha_3 = 0.15$, $\sum_{i=1}^{3} \alpha_i = 1$.

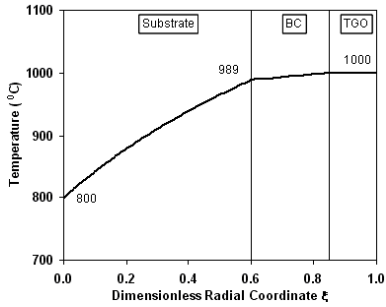

Fig. 4 – Temperature distribution in a multilayer thin circular plate used in the stress analysis

The thermal gradient in the plate induces the thermal stresses. In the present study, it was accepted that $\sigma_z = 0$ in a thin plate. Additionally, calculations have shown that the tangential stress is much larger than the radial stress. Therefore, the comparative study (Fig. 5, a-c) is performed only for the tangential stress using both numerical approaches discussed above and the finite element solution given in [59]. It is seen (Fig. 5, a-c) that the results obtained using the plane stress theory, as well as, the refined plate theory are in good agreement with the reference solution.

There is also an excellent agreement (Fig. 5, b, c) between the results generated by these two numerical approaches considered in the present study.

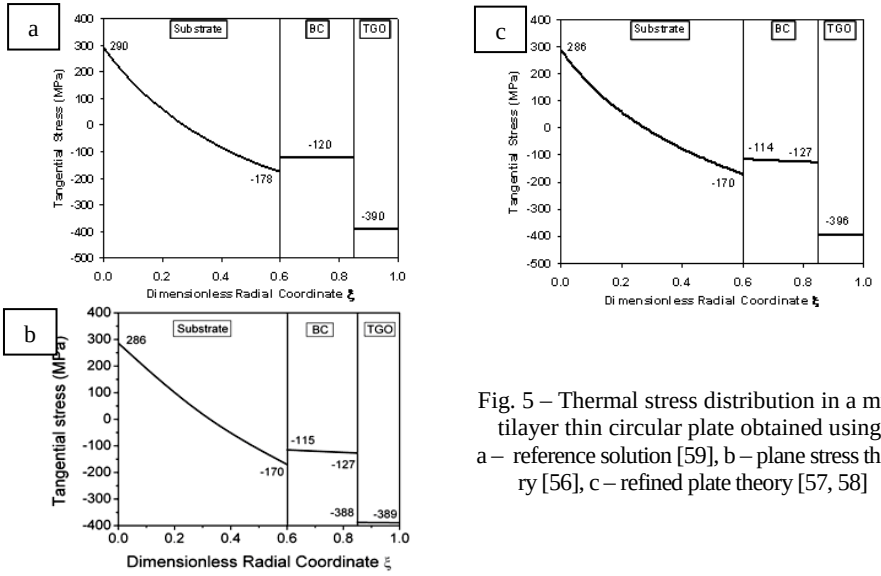

Fig. 5 – Thermal stress distribution in a multilayer thin circular plate obtained using: a – reference solution [59], b – plane stress theory [56], c – refined plate theory [57, 58]

5. Reference solution for hollow cylinder. As a second example for the verification of the two approaches used in the present paper, the multilayer long hollow cylinder (Fig. 1) with a = 2 mm and b = 4.3403 mm consisted of Ni-based superalloy substrate, the BC, the TGO and the BC is considered [37, 50]. The thickness of each layer is given in Table 2. In the following, the thermoelastic deformations of the cylinder subjected to an axial tensile load q =100 MPa distributed uniformly over the end, $q = N/[\pi(b^2 - a^2)]$, as well as, to the temperature T_a = 800°C on the inside and the temperature T_b = 1000°C on the outside of its walls (Fig. 6) will be analyzed. Creep of a cylinder is not considered here. The temperature at the reference state was taken as deposition temperature of the coating, i.e. T_{ref} = 1000 °C. The properties of each layer are defined in Tables 3 and 4.

Table 2 – **Materials and thickness of layers used for the calculations of thermal stresses in a long hollow cylinder plate**

Layer	Material	Thickness (mm)
Substrate	IN 100 DS	2.0
BC	NiCoCrAlY	0.120
TGO	Al_2O_3	0.0003
TC	7-8 YSZ	0.220

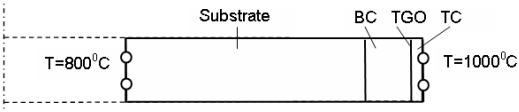

Fig. 6 – An axisymmetric slice of the coating hollow cylinder and thermal boundary conditions

Table 3 – **Properties for the TBC materials used in the analysis of thermal stresses in a multilayer long hollow cylinder at** $20\,^{\circ}\mathrm{C}$ (T_R) **and** $1000\,^{\circ}\mathrm{C}$ (T_H)

Layer	Elastic modulus (GPa)		Poisson's ratio		Thermal xpansion coefficient $\times 10^6$ (C^{-1})		Thermal conductivity (W/m/°C)	
	T_R	T_H	T_R	T_H	T_R	T_H	T_R	T_H
Bond coat	140	70	0.322	0.351	8.6	16.6	8.7	27.5
TGO	360	340	0.24	0.24	6.0	8.7	23	5.0
Top coat	13	16	0.22	0.28	9.0	11.5	1.88	1.6

Table 4 –**Material properties for the IN 100 DS substrate at** $20\,^{\circ}\mathrm{C}$ (T_R) **and** $1000\,^{\circ}\mathrm{C}$ (T_H) **used for the calculations of thermal stresses in a multilayer long hollow cylinder**

Radial elastic Modulus (GPa)		Axial elastic Modulus (GPa)		Poisson's ratio ν_0		Thermal expansion coefficient $\times 10^6$ (C^{-1})		Thermal conductivity (W/m/°C)	
T_R	T_H	T_R	T_H	T_R	T_H	T_R	T_H	T_R	T_H
215	148	120	80	0.3	0.3	11.5	18.8	15	30

Let T_i be the temperature (Fig. 7) in the $i-$th layer of a cylinder under consideration, r_{i-1} and r_i be the inner and outer radii of the $i-$th layer, and h_i be the thickness of the $i-$th layer, $i=\overline{1,4}$. It is obvious that $r_0 = a$, $r_4 = b$ and $r_i = r_{i-1} + h_i$.

The steady state heat conduction equation for the $i-$th layer can be written as

$$\frac{\partial^2 T_i}{\partial r^2} + \frac{1}{r}\frac{\partial T_i}{\partial r} = 0\,,\ r \in (r_{i-1}; r_i)\,,\ i=\overline{1,4}\,. \qquad (8)$$

The boundary conditions are given as follows

$$T_1 = T_a\,,\ r = a \qquad (9)$$

and

$$T_4 = T_b\,,\ r = b\,. \qquad (10)$$

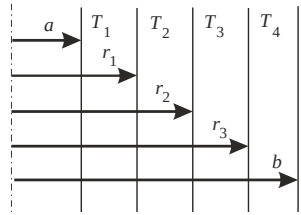

Fig. 7 – Schematic representation of the temperature field in a multilayer hollow cylinder

The continuity conditions for temperature and heat flux can be written as

$$T_i = T_{i+1}\,,\ r = r_i\,,\ i=\overline{1,3} \qquad (11)$$

and

$$K_i \frac{\partial T_i}{\partial r} = K_{i+1}\frac{\partial T_{i+1}}{\partial r}\,,\ r = r_i\,,\ i=\overline{1,3}\,, \qquad (12)$$

where K_i is the thermal conductivity of the $i-$th layer.

The analytical solution of the boundary value problem given by Eqs. (8)-(12) has the form [60]

$$T_1(r) = [(T_b - T_a)K_2K_3K_4 \ln(r/r_0) + T_a\Delta]/\Delta,$$
$$T_2(r) = [(T_b - T_a)K_1K_3K_4 \ln(r/r_1) + T_a(R_2 + R_3 + R_4) + T_bR_1]/\Delta,$$
$$T_3(r) = [(T_b - T_a)K_1K_2K_4 \ln(r/r_2) + T_a(R_3 + R_4) + T_b(R_1 + R_2)]/\Delta, \qquad (13)$$
$$T_4(r) = [(T_b - T_a)K_1K_2K_3 \ln(r/r_3) + T_aR_4 + T_b(R_1 + R_2 + R_3)]/\Delta,$$

where $\Delta = R_1 + R_2 + R_3 + R_4$, $R_1 = K_2K_3K_4 \ln(r_1/r_0)$, $R_2 = K_1K_3K_4 \ln(r_2/r_1)$, $R_3 = K_1K_2K_4 \ln(r_3/r_2)$, $R_4 = K_1K_2K_3 \ln(r_4/r_3)$.

The distribution of the temperature in the multilayer hollow cylinder under study at the steady state is shown in Fig. 8. It was calculated using Eq. (13) with the numerical data for the thermal conductivities K_i of the layers ($i = \overline{1,4}$) taken as the material constants at 900 °C. These values were found by linear interpolation using the data given in Tables 3 and 4. In this way, a common formula is used, such as

$$F(T) = F_1 + F_2 \cdot T, \; F_1 = \frac{T_2 \cdot F(T_1) - T_1 \cdot F(T_2)}{T_2 - T_1}, \; F_2 = \frac{F(T_2) - F(T_1)}{T_2 - T_1}, \qquad (14)$$

where $T \in [T_1, T_2]$, T_1 = 20 °C, T_2 = 1000 °C and function F plays the role of the thermal conductivities K_i of the layers. The dimensionless coordinate in the $i-$th layer of a cylinder in Fig. 8 has been defined by Eq. 7 ($i = \overline{1,4}$). Here it is assumed that $\alpha_0 = 0$, $\alpha_1 = 0.5$, $\alpha_2 = 0.18$, $\alpha_3 = 0.12$, $\alpha_4 = 0.2$ and $\sum_{i=1}^{4} \alpha_i = 1$.

The substrate material of this study is the Ni-based superalloy IN 100 which was directionally solidified (DS) with the [100] direction of the elongated grains approximately in the axial direction of the cylinder [37, 50]. In this case the elastic modulus in the radial direction of the specimen is approximately twice as high as the analogous magnitude in the axial direction (Table 4). Thus, the deviation in the grain orientation is attributed to the variation in the elastic deformation and the anisotropy of the Young's modulus. Therefore, the components of the elastic strain in the IN 100 DS substrate are defined by means of elastic compliances a_{ij} (i, j = 1, 2, 3) by the generalized Hooke's law for the orthotropic materials, such as [61]

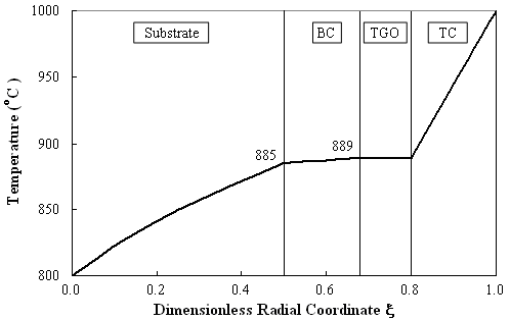

Fig. 8 – Temperature distribution in the coating hollow cylinder used in the stress analysis

$$\varepsilon_r^e = a_{11}\sigma_r + a_{12}\sigma_\theta + a_{13}\sigma_z\,,\ \varepsilon_\theta^e = a_{12}\sigma_r + a_{22}\sigma_\theta + a_{23}\sigma_z\,,$$
$$\varepsilon_z^e = a_{13}\sigma_r + a_{23}\sigma_\theta + a_{33}\sigma_z\,. \qquad (15)$$

Assuming transversal isotropy, elastic compliances have been determined in the present study as follows

$$a_{11} = a_{22} = E_r^{-1},\ a_{33} = E_z^{-1},\ a_{12} = a_{13} = a_{23} = -\nu_0 E_r^{-1} = -\nu_1 E_z^{-1}, \qquad (16)$$

where E_r and ν_0 are Young's modulus and Poisson's ratio under loading in the radial direction of the cylinder, and E_z and ν_1 are Young's modulus and Poisson's ratio under loading in the axial direction. Thus, the elastic compliances for the substrate can be calculated at each temperature T using Eq. (16), the values of the elastic constants at 20°C and 1000°C given in Table 4 and the interpolation procedure defined by Eq. (14). It is clear that Eq. (15) has been used for the substrate in this example instead of Eq. (2).

The loading by an axial force N and a thermal gradient across the thickness of the wall induces the stress-strain state in a cylinder. The numerical analysis using both approaches discussed above and the finite element solution given in [37, 50] have shown that the tangential and axial stresses in this example are much larger than the radial stress. It is seen (Figs. 9, b, c and 10, b, c) that the results obtained by the use of the generalized plane strain theory are in good agreement with the analogous ones com puted using the refined shell theory. Some disagreements with the reference solution in the TGO (Figs. 9. a-c and 10, a-c) can be explained by differences in the temperature distributions used in the stress calculations. The comparative study of the axial stresses in a cylinder with q = 100 MPa and q = 0 (Fig. 9, a-c) shows the strong influence of the tensile load. On the other hand, the influence of the load q on the tangential stresses is insignificant (Fig. 10, a-c). The relationship observed in the present study between the axial force and the deformation in the TBC system is in correlation with available experimental data [30, 62, 63].

6. Creep data. Now the creep deformation of the DLR test multilayer hollow cylinder (Fig. 1) with a = 2 mm and b = 4.3403 mm subjected to an axial tensile load q = 400 MPa distributed uniformly over the end, as well as, to a temperature T_a = 800 °C on the inside and a temperature T_b = 1000 °C on the outside of its walls (Fig. 6) is considered. The value of q = 400 MPa has been accepted according to the practical recommendations given in [64]. Further, the EB-PVD TBC system with the René 80 substrate, the NiCoCrAlY BC, the alumina TGO and the 8YSZ TC will be analyzed. Earlier this TBC system has been investigated experimentally in [65] while the TBC system involving the René N5 substrate has been studied experimentally in [6]. The thickness of each layer of the cylinder under consideration is given in Fig. 1. The assumption of the initial isotropy for the layer materials is accepted. The thermal conductivities for the substrate, the BC, the TGO and the BC are the same as those in Tables 3 and 4. Thus, the stationary distribution of the temperature in the present cylinder, as well as in the cylinder considered in the preceding section 2.4, is shown in Fig. 8.

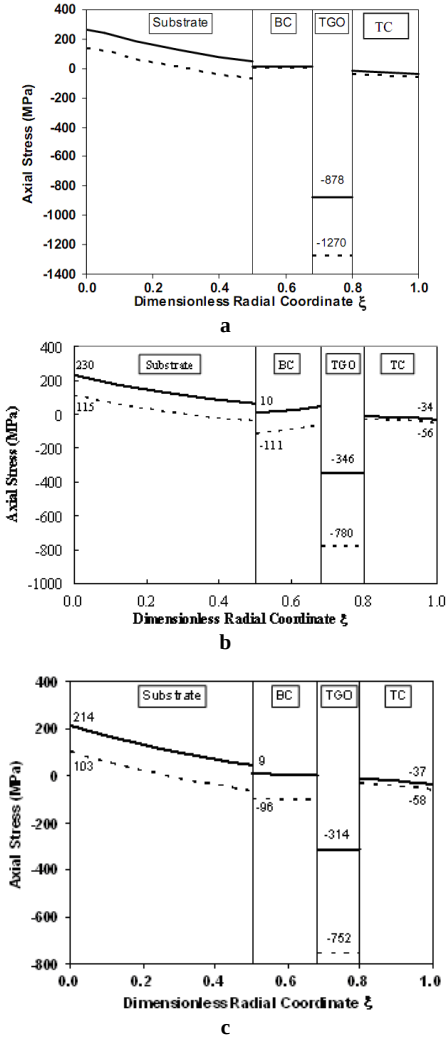

Fig. 9 – Axial stress distribution in a multilayer hollow cylinder obtained using (a) reference solution [37], (b) plane strain theory [56] and (c) refined shell theory [57, 58]. Predictions for axial load q =100 MPa are shown by solid line while the results for q = 0 are shown by dashed line

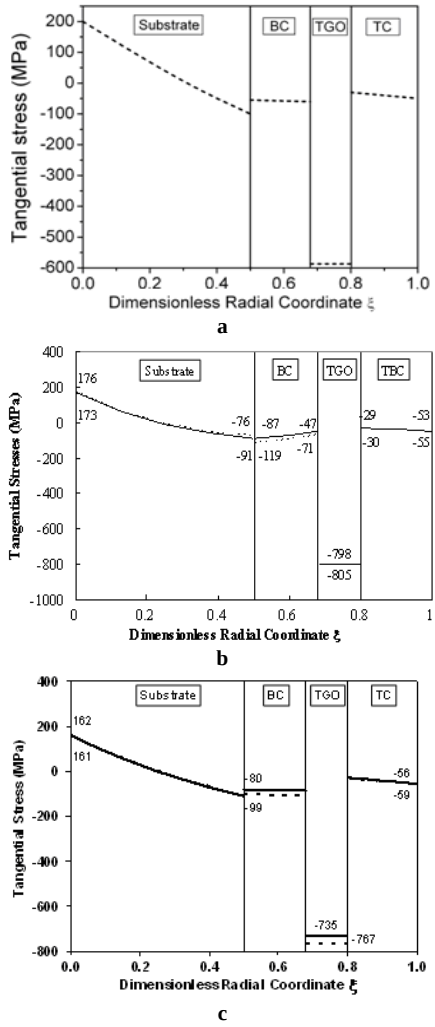

Fig. 10 – Tangential stress distribution in a multilayer hollow cylinder obtained with use of (a) reference solution [50], (b) plane strain theory [56] and (c) refined shell theory [57, 58]. Predictions for axial load q =100 MPa are shown by solid line while the results for q = 0 are shown by dashed line

The elastic parameters and thermal expansion coefficients of the layer materials in this study are presented in Table 5. The temperature at the reference state is the

deposition temperature of the coating, i.e. T_{ref} = 1000 °C.

Table 5 – **Elastic and thermal properties for the TBC materials used in the creep analysis of a multilayer long hollow cylinder**

Property	René 80 [66, 67]	BC [68]	TGO [37]	TC [37]
	800°C…900°C	850°C…950°C	20°C…1000°C	20°C…1000°C
Elastic modulus (GPa)	145.804…128.561	146.458…146.457	360…340	13…16
Poisson's ratio	0.3…0.3	0.3474…0.3495	0.24…0.24	0.22…0.28
Thermal expansion coefficient $\times 10^6$ (C^{-1})	15.1…16.0	15.4…16.2	6.0…8.7	9.0…11.5

Table 6 – **Parameters in the approximation of the creep curves given by Eq. (6) for the TBC materials used in the creep analysis of a multilayer long hollow cylinder**

Creep parameter	René 80 [66, 69]	BC [68]	TGO [70]	TC [30, 33]
	760°C…982°C	850°C…950°C	887°C…950°C	700°C…1000°C
$A\cdot 10^p$ ($\text{MPa}^{-n}\,\text{min}^{-m}$)	1.950…1.361	2.059…1.437	1.434…1.737	1.500…1.542
n	7.397…2.324	5.1…4.7	4.0…4.0	1.59…1.30
m	0.2577…0.2044	1…1	1…1	1…1
p	23…8	14…12	18…17	19…6

The creep curves of the René 80, the BC, the TGO and the BC under uniaxial tension can be described by Eq. (6) with the material parameters given in Table 6. In other words, the creep behavior of the materials at the temperatures T_1 and T_2 can be defined by the expressions $\varepsilon_z^c = A_1 t^{m_1} \sigma^{n_1}$ and $\varepsilon_z^c = A_2 t^{m_2} \sigma^{n_2}$, respectively. Then the creep deformation of the layer materials in the uniaxial case at the temperature $T \in [T_1, T_2]$ can be determined with use of Eq. (6) and an interpolation procedure, such as

$$A = A_1^{1-r} A_2^r,\ m = (1-r)m_1 + r m_2,\ n = (1-r)n_1 + r n_2, \qquad (17)$$

where $r = \eta \dfrac{T_2}{T}$ and $\eta = \dfrac{T - T_1}{T_2 - T_1}$. Thus, Eq. (4) corresponds to the creep constitutive equation in a TBC under multiaxial loading with creep parameters defined at the temperature $T \in [T_1, T_2]$ by Eq. (17).

7. Numerical analysis of creep for TBC system. Taking into account the good correlation obtained earlier in Sections 4 and 5 between the results generated by the two numerical approaches involved in the present paper, the numerical analysis of the influence of the creep deformation on the stress state in the TBC system under consideration

was performed with the use of the refined creep theory of moderately thick shells of revolution. In this way, in order to satisfy the condition of the generalized plane strain deformation, the length of the cylindrical segment (Fig. 1) in the numerical study using the refined shell theory was taken as $L = 10^{-17}$ mm, and, addi-tionally, symmetry boundary conditions have been applied.

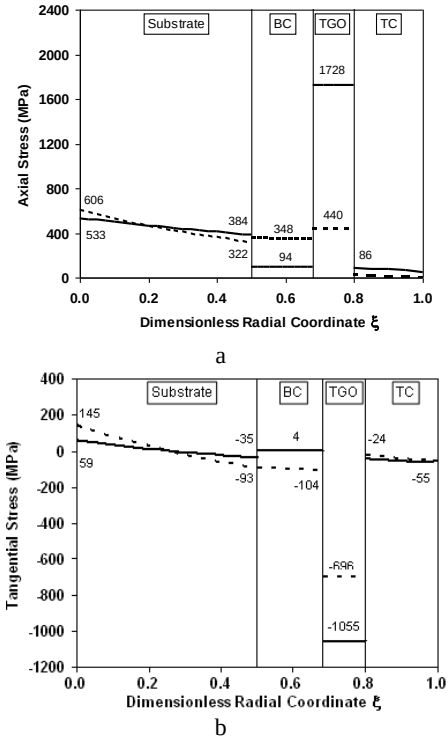

Fig. 11 – Redistribution of (a) axial and (b) tangential stresses in a multilayer hollow cylinder under creep deformation of the substrate, the BC, the TGO and the TC. Thermoelastic solution is shown by dashed line while stresses after 2 min are shown by solid line

The plot for stresses in the TBC system under study has a complex character (Fig. 11, a, b). The dimensionless coordinate in the i – th layer of a cylinder used in Fig. 11, a, b has been defined earlier in Section 5. The maximum tensile stress in a TBC system associated with the thermoelastic deformation is the axial stress at the inner surface of the tubular substrate. On the other hand, the maximum compressive stress related to the thermoelastic deformation of a multilayer hollow cylinder is the tangential stress in the TGO. The influence of the creep deformation on the stress state in the TBC system under consideration is significant. The maximum values of axial and tangential stresses after 2 min of creep have occurred in the TGO (Fig. 11, a, b). In this regard, the tensile stress and compressive one in the oxide under creep conditions have been found to be approximately equal to 1.7 GPa and 1 GPa, respectively.

A number of comments need to be made in reference to the stresses after 2 min of creep calculated in the TGO. First, a phenomenon related to the appearance and evolution of the growth stresses in the oxide is broadly discussed in the literature [11]. Thus, the growth stresses in the TGO can be caused not only by the high temperature oxidation, but also by the creep deformation that occurred in the TBC system. Second, the residual stress in the TGO determined by the luminescence spectroscopy method ranges usually from 1 to 5 GPa in compression [71, 72]. However, in some TBC systems the residual stress in the oxide can reach up to 1.5 GPa in tension [72]. Thus, there is a good correlation between the experimental data and model predictions obtained in the present paper. Third, a high level of

stresses in the oxide can be a source of failure at the interface between the BC and the TGO or between the TC and the TGO [11, 73]. Therefore, the magnitudes of these stresses are of critical importance for evaluating the lifetime of the TBC system.

8. Numerical simulation and discussion. The goal of the numerical modeling discussed in this section is to investigate the contribution of the creep properties of each layer into the stress redistribution in the TBC system under consideration with time. In this regard, some layers of a hollow cylinder under study are assumed to deform only thermoelastically while others also demonstrate creep deformation. Thus, involving creep of layers by step to step into the simulation of creep behavior the numerical study of the TBC stress redistribution will be performed and summarized.

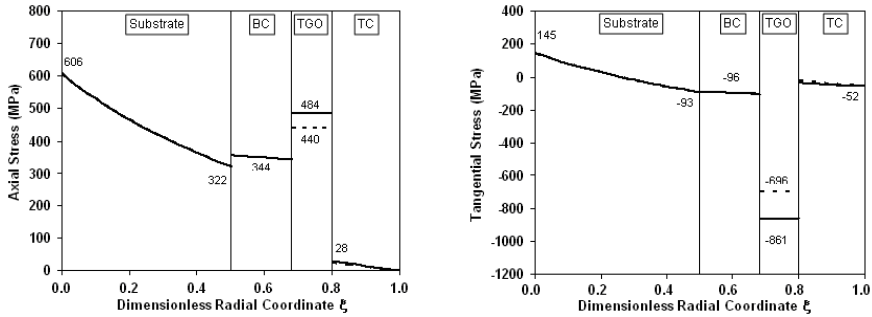

a b

Fig. 12 – Redistribution of (a) axial and (b) tangential stresses in a multilayer hollow cylinder under creep of the TGO and the TC, and thermoelastic deformation of the substrate and the BC. Thermoelastic solution for a cylinder is shown by dashed line while stresses after 2 min are shown by solid line

Let the TGO and the TC in the TBC system demonstrate creep deformation while the substrate and the BC will experience only thermoelastic deformation. The influence of creep on the stress state in the multilayer hollow cylinder under consideration is illustrated in Fig. 12, a, b. It is seen that visible stress redistribution with time occurs only in the oxide while the stresses in the substrate, the BC and the TC remain practically unchanged. Such factors as sintering of the YSZ, porosity of the zirconia top layer and elastic anisotropy of the TC may give rise to considerably higher stresses [74-79], and, therefore, more visible influence of creep on the stress state in this TC may be obtained by the numerical analysis. However, these issues will be a subject for future research.

The new numerical simulation refers to the case of a TBC system in which the BC, the TGO and the TC reveal creep behavior while the substrate shows only a thermoelastic response. It can be concluded from Fig. 13, a, b that in the present study the changing of stresses with time is visible in the BC and the TGO. On the other hand, these changes in the substrate and the TC tend to be numerically insignificant.

The next case of the numerical analysis is related to a TBC system in which the substrate, the TGO and the TC demonstrate creep while the BC will experience only thermoelastic deformation. It is known that the axial stress at the inner surface of the tubular substrate is the greatest in

the problem under consideration after the thermoelastic deformation of a cylinder. It is seen (Fig. 14, a) that although this stress is reduced during the creep process, the axial stress at the inner surface of the tubular substrate is still relatively high after 2 min of creep. However, the maximum tensile stress after 2 min of creep occurs in the TGO (Fig. 14 a). In general, the redistribution of stresses with time in the present study is significant in each layer of a TBC system (Fig. 14, a, b).

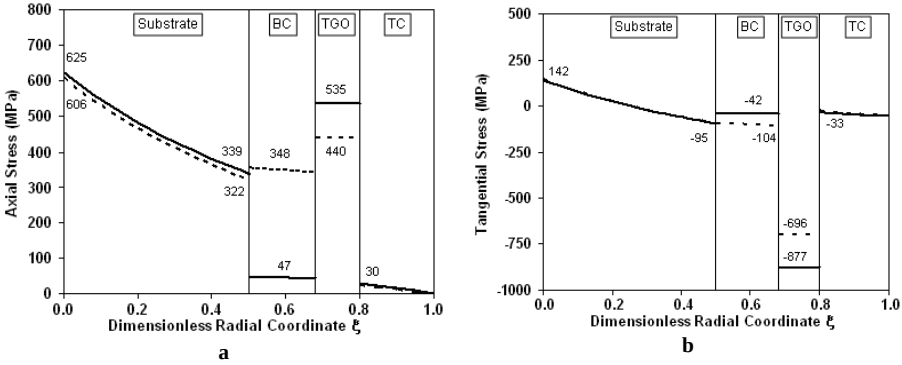

Fig. 13 – Redistribution of (a) axial and (b) tangential stresses in a multilayer hollow cylinder under creep of the BC, the TGO and the TC, and thermoelastic deformation of the substrate. Thermoelastic solution for a cylinder is shown by dashed line while stresses after 2 min are shown by solid line

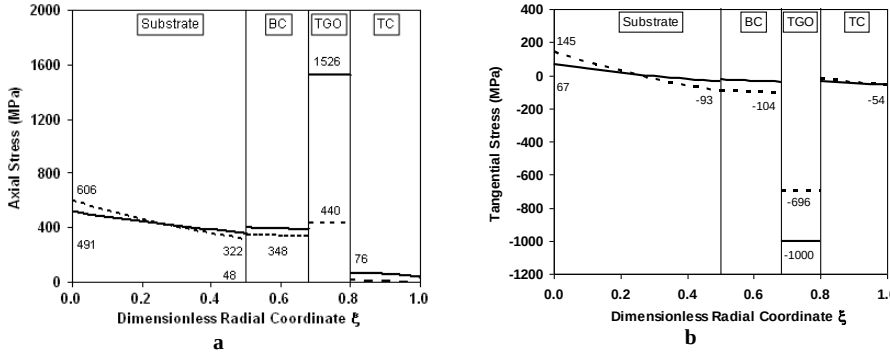

Fig. 14 – Redistribution of (a) axial and (b) tangential stresses in a multilayer hollow cylinder under creep of the substrate, the TGO and the TC, and thermoelastic deformation of the BC. Thermoelastic solution for a cylinder is shown by dashed line while stresses after 2 min are shown by solid line

Further numerical simulation refers to the case of a TBC system in which the substrate, the BC and the TGO demonstrate creep behavior while the TC shows only a thermoelastic response. The results of the numerical analysis are plotted in Fig. 15, a, b. The changing of stresses with time in this study, as well as, in the previous case is essential in each layer of a cylinder. In contrast, a significant relaxation of the axial stress under creep conditions occurs in a BC of the TBC system under consideration (Fig. 15, a).

A summary of the creep simulations is presented in Fig. 16, a, b. It is clear that creep of the substrate is the most important phenomenon that has the strong influence on the evolution of the growth stresses in the oxide and, consequently, durability of the TBC system under study. Hence, the influence of the creep deformation of the oxide and the YSZ BC on the stress state in the TGO is insignificant.

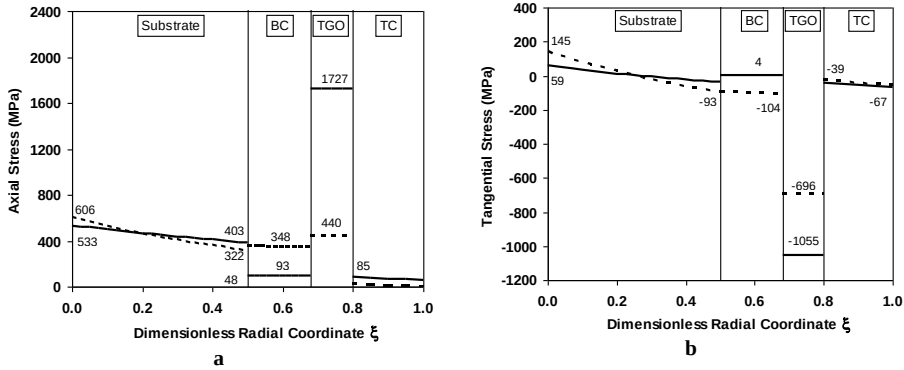

a b

Fig. 15 – Redistribution of (a) axial and (b) tangential stresses in a multilayer hollow cylinder under creep of the substrate, the BC and the TGO, and thermoelastic deformation of the TC. Thermoelastic solution for a cylinder is shown by dashed line while stresses after 2 min are shown by solid line

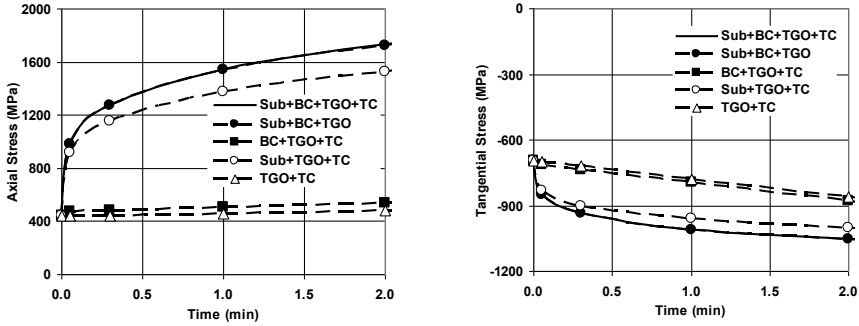

a b

Fig. 16 – Time variation of (a) axial and (b) tangential stresses in the TGO of a multilayer hollow cylinder. Layers demonstrating the creep behavior in simulations are indicated next to the mentioned lines in the field of both diagrams in each case of the numerical analysis

9. Conclusions. In this paper, two different numerical approaches have been presented to find the stress redistribution in TBC systems for a Ni-based superalloy substrate under creep conditions. For this purpose, the creep deformation of the multilayer hollow cylinder subjected to an axial tensile load distributed uniformly over the end and a temperature gradient through the wall has been analyzed. Hence, the loading and creep conditions simulate the conditions which may occur in-service and limit the per-

formance of turbine blades as close as possible. A number of reference solutions obtained by other authors and by other methods have been used for the structural analysis. It was established numerically that creep of the Ni-based superalloy substrate is responsible for the evolution of the growth stresses in the oxide of the TBC system under study. Thus, the effectiveness of coating is closely related to the creep properties and composition of the substrate. The creep problems presented in this paper should be considered as structural benchmarks by users of commercial software packages to verify the finite element analysis of stress redistribution in coatings at high temperatures.

This research was partially supported by the German Academic Exchange Service (DAAD), the Alexander von Humboldt Stiftung and the German Federal Ministry of Education and Research (BMBF) through the German Aerospace Center (DLR).

References: 1. *R.A. Miller*. Current status of thermal barrier coatings–an overview. // Surf. Coat. Technol. –1987. – Vol. 30. –№ 1. – PP. 1-11. **2**. *U. Schulz, K. Fritscher, C. Leyens, M. Peters, W.A. Kaysser*. Thermocyclic behavior of differently stabilized and structured EB-PVD thermal barrier coatings. // Mat.-wiss. u. Werkstofftech. –1997. –Vol. 28. –№ 8. –PP. 370-376. **3.** *D. Stöver, C. Funke.* Directions of the development of thermal barrier coatings in energy applications. // J. Mater. Process. Technol. –1999. –Vol. 92–93. –PP. 195–202. **4**. *N. P. Padture, M. Gell, E. H. Jordan.* Thermal barrier coatings for gas-turbine engine applications. // Science. – 2002. – Vol. 296. – № 5566. – PP. 280-284. **5**. *K. Fritscher, U. Schulz, C. Leyens*. Lifetime-determining spalling mechanisms of NiCoCrAlRE / EB-PVD zirconia TBC systems. // Mat.-wiss. u. Werkstofftech. – 2007. – Vol. 38. – № 9. – PP. 734-746. **6**. *C. Leyens, U. Schulz, B.A. Pint, I.G. Wright*. Influence of electron beam physical vapor deposited thermal barrier coating microstructure on thermal barrier coating system performance under cyclic oxidation conditions. // Surf. Coat. Technol. – 1999. – Vol. 120. – PP. 68-76. **7**. *K. Fritscher, C. Leyens.* Grenzschichtproblematik und Haftung von EB-PVD-Wärmedämmschichtsystemen, Mat.-wiss. u. Werkstofftech. –1997. –Vol. 28. –№ 8. –PP. 384-390. **8**. *M. Peters, C. Leyens, U. Schulz, W.A. Kaysser*. EB-PVD thermal barrier coatings for aeroengines and gas turbines. // Adv. Eng. Mater. –2001. –Vol. 3. –№ 4. –PP. 193-204. **9**. *R. Vaßen, F. Cernuschi, G. Rizzi, A. Scrivani, N. Markocsan, L. Östergren, A. Kloosterman, R. Mevrel, J. Feist, J. Nicholls*. Recent activities in the field of thermal barrier coatings including burner rig testing in the European Union. // Adv. Eng. Mater. –2008. –Vol. 10. –№ 10. –PP. 907-921. **10**. *M.F.J. Koolloos , G. Marijnissen.* Burner Rig Testing of "Herringbone" EB-PVD Thermal Barrier Coatings. Report № NLR-TP-2002-293.– Lomm: National Aerospace Laboratory, The Netherlands. – 2002. **11**. *A.G. Evans, D.R. Mumm, J.W. Hutchinson, G.H. Meier, F.S. Pettit.* Mechanisms controlling the durability of thermal barrier coatings. // Prog. Mater. Sci. – 2001. – Vol. 46. – № 5. – PP. 505-553. **12**. *F. J. Cunha, M. T. Dahmer, M. K. Chyu*. Thermal-mechanical life prediction system for anisotropic turbine components. // Trans. ASME. J. Turbomach. –2006. –Vol. 128. –№ 2. –PP. 240-250. **13**. *A. Zolochevsky, N. Sergienko, S. Eremenko, A. Kühhorn*. Constitutive and numerical modeling of chemical and mechanical phenomena in thermal barrier coatings for gas turbine blades of aircraft engines. // Вестник НТУ „ХПИ". Тем. вып.: „Транспортное машиностроение". – Харьков: НТУ "ХПИ".– 2010.– № 38. -С. 99 -109. **14**. *M. Caliez, F. Feyel , S. Kruch, J.-L. Chaboche.* Oxidation induced stress fields in an EB-PVD thermal barrier coating. // Surf. Coat. Technol. –2002. –Vol. 157. –№ 2. –PP. 103-110. **15**. *M. Caliez, J.-L. Chaboche, F. Feyel, S. Kruch*. Numerical simulation of EBPVD thermal barrier coatings spallation. // Acta Mater. – 2003. – Vol. 51. – № 4. –PP. 1133-1141. **16**. *A. M. Karlsson, J. W. Hutchinson, A. G. Evans.* The displacement of the thermally grown oxide in thermal barrier systems upon temperature cycling. // Mater. Sci. Eng. –2003. –Vol. A 351. –№ 1. –PP. 244-257. **17.** *R.W. Steinbrech, V. Postolenko, J. Mönch, J. Malzbender , L. Singheiser*. Testing method to assess lifetime of EB-PVD thermal barrier coatings on tubular specimens in static and cyclic oxidation tests. // Ceramics Int. –2011. –Vol. 37. – № 1. – PP. 363-368. **18**. *S. Dryepondt, D. R. Clarke*. Effect of superimposed uniaxial stress on rumpling of platinum-modified nickel aluminide coatings. // Acta Mater. –2009. –Vol. 57. –№ 7. –PP. 2321-2327. **19**. *V. G. Karaivanov*. Lifetime Prediction Modeling of Airfoils for Advanced Power Generation. PhD thesis. – Pittsburgh: University of Pittsburgh, The USA. – 2009. **20**. *R. Kitazawa, M. Tanaka, Y. Kagawa, Y.F. Liu*. Damage evolution of TBC system under in-phase thermo-mechanical tests. // Mater. Sci. Eng. –2010. –Vol. B 173. –№ 1. –PP. 130-134. **21**. *F. Gallerneau, J.-L. Chaboche*. Fatigue life prediction of single crystals for turbine blade applications. // Int. J. Damage Mech. –1999. –Vol. 8. –№ 4. –PP. 404-427. **22**. *B. Baufeld, M. Bartsch, M. Heinzelmann*. Advanced thermal gradient mechanical fatigue testing of CMSX-4 with an oxidation protection coating. // Int. J. Fatigue. –2008. –Vol. 30. –№ 2. –

PP. 219-225. **23**. *M.T. Hernandez, D. Cojocaru, M. Bartsch, A.M. Karlsson*. On the opening of a class of fatigue cracks due to thermo-mechanical fatigue testing of thermal barrier coatings. // Comp. Mater. Sci. –2011. –Vol. 50. –№ 9. –PP. 2561-2572. **24**. *N.A. Fleck, Th. Zisis*. The erosion of EB-PVD thermal barrier coatings: The competition between mechanisms. // Wear. –2010. –Vol. 268. –№ 11. –PP. 1214-1224. **25**. *F. Cernuschi, L. Lorenzoni, S. Capelli, C. Guardamagna, M. Karger, R. Vaßen, K. von Niessen, N. Markocsan, J. Menuey, C. Giolli*. Solid particle erosion of thermal spray and physical vapour deposition thermal barrier coatings. // Wear. –2011. –Vol. 271. –№ 11. –PP. 2909-2918. **26**. *P.K. Wright, A.G. Evans*. Mechanisms governing the performance of thermal barrier coatings. // Current Opinion Solid State Mater. Science. 1999. –Vol. 4. –№ 3. –PP. 255-265. **27**. *R.T. Wu, R.C. Reed*. On the compatibility of single crystal superalloys with a thermal barrier coating system. // Acta Mater. –2008. –Vol. 56. –№ 3. –PP. 313-323. **28**. *V. Teixeira*. Mechanical integrity in PVD coatings due to the presence of residual stresses. // Thin Solid Films. – 2001. –Vol. 392. –№ 2. –PP. 276-281. **29**. *M. Białas*. Finite element analysis of stress distribution in thermal barrier coatings. // Surf. Coat. Technol. –2008. –Vol. 202. –№ 24. –PP. 6002-6010. **30**. *A.M. Freborg, B.L. Ferguson, W.J. Brindley, G.J. Petrus*. Modeling oxidation induced stresses in thermal barrier coatings. // Mater. Sci. Eng. –1998. –Vol. A 245. –№ 2. –PP. 182-190. **31**. *E. Tzimas, H. Müllejans, S.D. Peteves, J. Bressers, W. Stamm*. Failure of thermal barrier coating systems under cyclic thermomechanical loading. // Acta Mater. –2000. –Vol. 48. –№ 18–19. –PP. 4699-4707. **32**. *J. Rösler, M. Bäker, M. Volgmann*. Stress state and failure mechanisms of thermal barrier coatings: role of creep in thermally grown oxide. // Acta Mater. –2001. –Vol. 49. –№ 18. –PP. 3659-3670. **33**. *Y. Liu, C. Persson, J. Wigren*. Experimental and numerical life prediction of thermally cycled thermal barrier coatings. // J. Thermal Spray Technol. –2004. –Vol. 13. –№ 3. –PP. 415-424. **34**. *J. Ding, F.-X. Li, K.-J. Kang*. Effects of material creep on displacement instability in a surface groove under thermo-mechanical cycling. // Surf. Coat. Technol. –2009. –Vol. 204. – № 1. –PP. 157-164. **35**. *Q.-Q. Chen, F.-Z. Xuan, S.-T. Tu*. Modeling of creep deformation and its effect on stress distribution in multilayer systems under residual stress and external bending. // Thin Solid Films. –2009. –Vol. 517. –№ 9. – PP. 2924-2929. **36**. *A.G. Evans, M.Y. He, A. Suzuki, M. Gigliotti, B. Hazel, T.M. Pollock*. A mechanism governing oxidation-assisted low-cycle fatigue of superalloys. // Acta Mater. –2009. –Vol. 57. –№ 10. –PP. 2969-2983. **37**. *M.T. Hernandez, A.M. Karlsson, M. Bartsch*. On TGO creep and the initiation of a class of fatigue cracks in thermal barrier coatings. // Surf. Coat. Technol. –2009. –Vol. 203. –№ 23. –PP. 3549-3558. **38**. *J. Schwarzer, D. Löhe, O. Vöhringer*. Influence of the TGO creep behavior on delamination stress development in thermal barrier coating systems. // Mater. Sci. Eng. –2004. –Vol. A 387–389.–PP. 692-695. **39**. *M.Y. Ali, S.Q. Nusier, G.M. Newaz*. Mechanics of damage initiation and growth in a TBC/superalloy system. // Int. J. Solids Struct. –2001. –Vol. 38. –№ 19. –PP. 3329-3340. **40**. *E.P. Busso, Z.Q. Qian, M.P. Taylor, H.E. Evans*. The influence of bondcoat and topcoat mechanical properties on stress development in thermal barrier coating systems. // Acta Mater. –2009. –Vol. 57. –№ 8. –PP. 2349-2361. **41**. *U. Hermosilla*. Mechanical Modelling of Thermal Barrier Coatings at High Temperatures. PhD thesis. –Nottingham: The University of Nottingham, UK. – 2008. **42**. *U. Hermosilla, M.S.A. Karunaratne, I.A. Jones, T.H. Hyde, R.C. Thomson*. Modelling the high temperature behaviour of TBCs using sequentially coupled microstructural–mechanical FE analyses. // Mater. Sci. Eng. –2009. –Vol. A 513–514. –PP. 302-310. **43**. *M. Ranjbar-Far, J. Absi, S. Shahidi, G. Mariaux*. Impact of the non-homogenous temperature distribution and the coatings process modeling on the thermal barrier coatings system. // Mater. Design. – 2011. – Vol. 32. – № 2. –PP. 728-735. **44**. *K.J. Bathe, G.A. Ledezma*. Benchmark problems for incompressible fluid flows with structural interactions. // Comput. Struct. –2007. –Vol. 85. –№ 11. –PP. 628-644. **45**. *A. Zolochevsky, A. Martynenko, A. Kühhorn*. Structural benchmark creep and creep damage testing for finite element analysis with material tension–compression asymmetry and symmetry. // Comput. Struct. –2012. –Vol. 100-101.–PP. 27-38. **46**. *A.A. Becker, T.H. Hyde, W. Sun, P. Andersson*. Benchmarks for finite element analysis of creep continuum damage mechanics. // Comput. Mater. Sci. –2002. –Vol. 25. –№ 1-2. – PP. 34-41. **47**. *O.J.A. Gonçalves Filho*. Benchmark for finite element analysis of stress redistribution induced by creep damage. // Comput. Mater. Sci. –2005. – Vol. 33. –№ 4. – PP. 419-428. **48**. *H. Altenbach, K. Naumenko, Y. Gorash*. Numerical benchmarks for creep - damage modeling. // PAMM. –2007. –Vol. 7. –№ 1. – PP. 4040021- 4040022. **49**. *D.L. Krause, S. Kalluri, R.R. Bowman, A.R. Shah*. Structural Benchmark Creep Testing for the Advanced Stirling Convertor Heater Head. Report № NASA/TM-2008-215435.– Glenn Research Center: NASA, The USA . – 2008. **50**. *B. Baufeld, M. Bartsch, S. Dalkiliç, M. Heinzelmann*. Defect evolution in thermal barrier coating systems under multi-axial thermomechanical loading. // Surf. Coat. Technol. –2005. –Vol. 200. –№ 5. –PP. 1282-1286. **51**. *M. Bartsch, G. Marci, K. Mull, C. Sick*. Fatigue testing of ceramic thermal barrier coatings for gas turbine blades. // Adv. Eng. Mater. –1999. –Vol. 1. –№ 2. – PP. 127-129. **52**. *H. Chen, A.R.S. Ponter*. Linear Matching Method on the evaluation of plastic and creep behaviours for bodies subjected to cyclic thermal and mechanical loading. // Int. J. Numer. Methods Eng. – 2006. – Vol. 68. – № 1. –PP. 13-32. **53**. *B. Baufeld, U. Schulz*. Life time dependency on the pre-coating treatment of a thermal barrier coating under thermal cycling. // Surf. Coat. Technol. –2006. –Vol. 201. –№ 6. –PP. 2667-2675. **54**. *M.K. Darabi, R.K. Abu*

Al-Rub, E.A. Masad, C.-W. Huang, D.N. Little. A thermo-viscoelastic–viscoplastic–viscodamage constitutive model for asphaltic materials. // Int. J. Solids Struct. –2011. –Vol. 48. –№ 1. –PP. 191-207. **55**. *A.A. Zolochevskii*. Effect of the type of loading on the creep of isotropic strain-hardening materials. // Sov. Appl. Mech. –1988. –Vol. 24. –№ 2. –PP. 185-191. **56**. *A. Zolochevsky, S. Sklepus, T.H. Hyde, A.A. Becker, S. Peravali*. Numerical modeling of creep and creep damage in thin plates of arbitrary shape from materials with different behavior in tension and compression under plane stress conditions. // Int. J. Numer. Methods Eng. –2009. –Vol. 80. –№ 11. –PP. 1406-1436. **57**. *A. Zolochevsky, A. Galishin, A. Kühhorn, M. Springmann*. Transversal shear effect in moderately thick shells from materials with characteristics dependent on the kind of stress state under creep-damage conditions: theoretical framework. // Techn. Mech. – 2009. –Vol. 29. –№ 1. –PP. 38-47. **58**. *A. Galishin, A. Zolochevsky, A. Kühhorn, M. Springmann*. Transversal shear effect in moderately thick shells from materials with characteristics dependent on the kind of stress state under creep-damage conditions: numerical modeling. // Techn. Mech. –2009. –Vol. 29. –№ 1. –PP. 48-59. **59**. *J. Shi, A.M. Karlsson, B. Baufeld, M. Bartsch*. Evolution of surface morphology of thermo-mechanically cycled NiCoCrAlY bond coats. // Mater. Sci. Eng. –2006. –Vol. A . 434. –№ 1. –PP. 39-52. **60**. *H.S. Carslaw, J.C. Jaeger*. Conduction of Heat in Solids, 2nd ed. – London: Oxford University Press. – 1959. **61**. А.А Золочевский, А.Н. Склепус, С.Н. Склепус. Нелинейная механика деформируемого твердого тела. – Харьков: Бізнес Інвестор Груп, 2011.– 720 с. **62**. *M. Bäker, J. Rösler, E. Affeldt*. The influence of axial loading on the interface stresses of thermal barrier coatings. // Comp. Mater. Sci. –2009. –Vol. 47. –№ 2. –PP. 466-470. **63**. *D.S. Balint, S.-S. Kim, Y.-F. Liu, R. Kitazawa, Y. Kagawa, A.G. Evans*. Anisotropic TGO rumpling in EB-PVD thermal barrier coatings under in-phase thermomechanical loading. // Acta Mater. –2011. –Vol. 59. –№ 6. –PP. 2544-2555. **64**. *M. Bartsch, B. Baufeld, M.* Heinzelmann, A. M. Karlsson, S. Dalkilic, L. Chernova. Multiaxial thermo - mechanical fatigue on material systems for gas turbines. // Mat.-wiss. u. Werkstofftech. –2007. –Vol. 38. –№ 9. –PP. 712-719. 65. R. Stolle. Conventional and Advanced Coatings for Turbine Airfoils. – München: MTU Aero Engines. – 2006. 66. V.S. Bhattachar, D.C. Stouffer. Constitutive equations for the thermomechanical response of Rene 80. Part 1: Development from isothermal data. // Trans. ASME. J. Eng. Mater. Technol. –1993. –Vol. 115. –№ 4. –PP. 351-357. **67**. *Z. Li, K.C. Mills*. The effect of γ′ content on the densities of Ni-based superalloys. // Metall. Mater. Trans. –2006. –Vol. B 37. –№ 5. –PP. 781-790. **68**. *J. Schwarzer, K.E. Rostek, T. Beck, D. Löhe, O. Vöhringer*. Modelling the stress state of a thermal barrier coating system at high temperatures. // Z. Metallkd. –2005. –Vol. 96. –№ 7. –PP. 718-724. **69**. *V.G. Ramaswamy, D.C. Stouffer, J.H. Laflen*. A unified constitutive model for the inelastic uniaxial response of Rene'80 at temperatures between 538 °C and 982 °C. // Trans. ASME. J. Eng. Mater. Technol. – 1990. –Vol. 112. –№ 3. –PP. 280-286. **70**. *B. W. Veal, A. P. Paulikas, P. Y. Hou*. Creep in protective α- Al_2O_3 thermally grown on β-NiAl. // Appl. Phys. Lett. –2007. –Vol. 90. –№ 12. –PP. 121914-1 - 121914-3. **71**. *G. Lee, A. Atkinson, A. Selçuk*. Development of residual stress and damage in thermal barrier coatings. // Surf. Coat. Technol. – 2006. –Vol. 201. –№ 7. –PP. 3931-3936. **72**. *A. Selcuk, A. Atkinson*. Analysis of the Cr^{3+} luminescence spectra from thermally grown oxide in thermal barrier coatings. // Mater. Sci. Eng. –2002. –Vol. A 335. –№ 1-2. –PP. 147-156. **73**. *M. Bartsch, B. Baufeld, S. Dalkilic, I. Mircea*. Testing and characterization of ceramic thermal barrier coatings. // Mater. Sci. Forum. –2005. –Vol. 492-493.–PP. 3-8. **74**. *E.F. Rejda, D.F. Socie, T. Itoh*. Deformation behavior of plasma-sprayed thick thermal barrier coatings. // Surf. Coat. Technol. –1999. –Vol. 113. –№ 3. –PP. 218-226. **75**. *V. Teixeira*. Numerical analysis of the influence of coating porosity and substrate elastic properties on the residual stresses in high temperature graded coatings. Surf. Coat. Technol. –2001. –Vol. 146 –147. –PP. 79-84. **76**. *E.P. Busso , Z.Q. Qian*. A mechanistic study of microcracking in transversely isotropic ceramic–metal systems. Acta Mater. –2006. –Vol. 54. – № 2. –PP. 325-338. **77**. *N. Zotov, M. Bartsch, L. Chernova, D.A. Schmidt, M. Havenith, G. Eggeler*. Effects of annealing on the microstructure and the mechanical properties of EB-PVD thermal barrier coatings. Surf. Coat. Technol. –2010. –Vol. 205. –№ 2. –PP. 452-464. **78**. *C. Eberl, D.S. Gianola, X. Wang, M.Y. He, A.G. Evans*. J. Hemker. A method for in situ measurement of the elastic behavior of a columnar thermal barrier coating. Acta Mater. – 2011. –Vol. 59. –№ 9. –PP. 3612-3620. **79**. *C. Pfeiffer, E. Affeldt, M. Göken*. Miniaturized bend tests on partially stabilized EB-PVD ZrO_2 thermal barrier coatings. Surf. Coat. Technol. –2011. –Vol. 205. –№ 10. – PP. 3245-3250.

Поступила в редколлегию 06.02.2013